Physics in Medicine & Biology

IPEM Institute of Physics and Engineering in Medicine

CrossMark

CORRIGENDUM

Corrigendum: Quantification of the trabecular bone volume fraction for bone marrow dosimetry in molecular radiotherapy by using a dual-energy (SPECT/)CT (2019 *Phys. Med. Biol.* **64** 205014)

Maikol Salas-Ramirez[1,4], Johannes Tran-Gia[1], Uwe Gbureck[2], Aleksander Kosmala[3] and Michael Lassmann[1]

[1] Department of Nuclear Medicine, University of Würzburg, Würzburg, Germany
[2] Department for Functional Materials in Medicine and Dentistry, University of Würzburg, Würzburg, Germany
[3] Department of Diagnostic and Interventional Radiology, University of Würzburg, Würzburg, Germany
[4] Author to whom any correspondence should be addressed.

E-mail: E_Salas_M@ukw.de

In table 5, two errors were identified:

1. Inverted labelling of the columns five and six.
2. There was a typo error of the values of VF_B^c in the spongiosa region.

The updated table 5 contains the corrected values.

Table 5. Values of mass and volume fractions of HA and bone in lumbar vertebrae 1 and 2 from a patient image set.

Region		Parameter					
		MF_{HA}	VF_{HA}	VF_B^b	MF_B	VF_B^c	$R_{HA/B}$
Whole vertebra[a]	Lumbar vertebra 1	0.138	0.052	0.124	0.249	0.148	0.554
	Lumbar vertebra 2	0.145	0.056	0.132	0.261	0.157	0.556
Spongiosa	Lumbar vertebra 1	0.113	0.039	0.093	0.203	0.110	0.557
	Lumbar vertebra 2	0.116	0.040	0.095	0.208	0.113	0.558

MF_{HA}: hydroxyapatite mass fraction. VF_{HA}: hydroxyapatite volume fraction. MF_B: bone mass fraction. VF_B: bone volume fraction.
[a] Excluding transverse processes.
[b] First volume fraction calculation method.
[c] Second volume fraction calculation method.

Physics in Medicine & Biology

IPEM Institute of Physics and Engineering in Medicine

CrossMark

PAPER

Quantification of the trabecular bone volume fraction for bone marrow dosimetry in molecular radiotherapy by using a dual-energy (SPECT/)CT

Maikol Salas-Ramirez[1], Johannes Tran-Gia[1], Uwe Gbureck[2], Aleksander Kosmala[3] and Michael Lassmann[1]

[1] Department of Nuclear Medicine, University of Würzburg, Würzburg, Germany
[2] Department for Functional Materials in Medicine and Dentistry, University of Würzburg, Würzburg, Germany
[3] Department of Diagnostic and Interventional Radiology, University of Würzburg, Würzburg, Germany

E-mail: E_Salas_M@ukw.de

Abstract

A complete characterization of spongiosa (bone marrow plus trabecular bone) is required to calculate the absorbed dose to active bone marrow. Due to the complex microanatomy, it is necessary to apply non-conventional imaging methods in nuclear medicine. The aim of this study is validating a phantomless quantification method using dual-energy quantitative computed tomography (DEQCT) for the quantification of trabecular bone volume fraction for bone marrow dosimetry in molecular radiotherapy.

First, a phantomless quantification method (mass fraction method) based on x-ray beam and detector sensitivity was validated in an integrated dual energy SPECT/CT and in a dual source computed tomography (DSCT) system for comparison. The validation was performed in a phantom consisting of different water, fat and hydroxyapatite compositions. Moreover, the European spine phantom (ESP) was used to simulate the spine geometry. Bone mineral content (BMC) of the whole vertebra and bone mineral density (BMD) in the spongiosa region of each phantom vertebra were measured using DEQCT and dual energy x-ray absorptiometry (DEXA). Lastly, BMC was measured in a patient using DEQCT and DEXA.

Measured values of hydroxyapatite fraction and nominal values in the homemade phantom showed a good correlation. The relative error remained below 14.2%. Quantification of BMC (in whole vertebra) and BMD (in spongiosa) in the ESP showed a good agreement between measured values and nominal values. The relative error remained between 0.7% and 7.5% for $BMC_{SPECT/CT}$, 1.1% and 7.7% for BMC_{DSCT}, 5.4% and 32.0 for $BMD_{SPECT/CT}$, and 59.4% and 10.0% for BMD_{DSCT}. Quantification of BMC in lumbar vertebrae 1 and 2 of a patient showed relative errors of 7.6% and -8.4% between DEXA and DSCT.

Our study shows that DEQCT using a mass fraction method (phantomless) enables quantification of hydroxyapatite in a clinical nuclear medicine setting. An overestimation of the hydroxyapatite volume fraction was observed in all quantified regions, in particular in the spongiosa region of ESP. This result might be related to insufficient information about the x-ray spectra and the detector sensitivity function.

Introduction

One of the main goals of treatment planning in molecular radiotherapy is to predict the level of toxicity caused by the radionuclide therapy in bone marrow (Hindorf *et al* 2010). Bone marrow is composed of three main compartments: red marrow, yellow marrow, and trabecular bone. These three compartments form a

microstructure with a highly complex spatial distribution. In addition, the volume fraction of each compartment is age- and gender-dependent (ICRP 1995, 2002, Salas-Ramirez *et al* 2018).

Red marrow and yellow marrow are equivalent to marrow cellularity and marrow fat fraction, respectively. This equivalency assumes that the volume occupied by non-hematopoietic cells and structures located in the red marrow (e.g. marrow support cells, vascular structures, marrow stromal cells and other cells) is small and difficult to measure in clinical settings (Bolch *et al* 2001). A definition of marrow cellularity was proposed by Bolch *et al* (2001) as the fraction of marrow space not occupied by adipocytes:

$$(\text{Marrow Cellularity}) \approx 1 - (\text{Fat Fraction}). \tag{1}$$

In a previous study (Salas-Ramirez *et al* 2018), we evaluated the feasibility of magnetic resonance imaging (MRI) for quantification of marrow fat fraction in patients. The study validated a non-invasive method for quantifying the fat fraction of bone marrow in a clinical setting.

A second step in the characterization of spongiosa in patients is the quantification of trabecular bone volume. Some studies (Bolch *et al* 2001, Wilderman *et al* 2013, Geyer *et al* 2017) have pointed out the necessity to quantify the trabecular bone volume fraction (fraction of bone marrow space occupied by trabecular bone). This parameter, which is typically referred to as TBVF, is a fundamental parameter in 3D dosimetry models of the trabecular skeleton (Bolch *et al* 2001, Shah *et al* 2005, Wilderman *et al* 2013, Geyer *et al* 2017). Wilderman *et al* (2013), applying a representative mathematical spongiosa model, found that, for marrow cellularities of 20%, 50% and 80%, the dose rates can differ by up to 10% as a function of bone volume. Geyer *et al* (2017), using micro-CT segmented images of trabecular bone and considering a relative change of $\pm 5\%, \pm 10\%$, and $\pm 15\%$ in trabecular bone volume fraction, observed a variability larger than $\pm 10\%$ for radionuclide S value in parietal bone, mainly due to the high proportion of trabecular bone in this bone site.

Bone tissue is composed of an organic matrix and inorganic salts (ICRP 1996, 2002). Quelch *et al* (1983) documented for an adult vertebra values of 66.3% mineral content and 33.7% organic content by weight lost during ashing. According to Neuman (1980), the inorganic component of bone principally consists of submicroscopic deposits of calcium phosphate forms, which are in transition to solid phase hydroxyapatite $[Ca_{10}(PO_4)_6(OH)_2]$.

Geyer *et al* (2017) proposed the use of dual-energy computed tomography (DECT) imaging to quantify the bone mineral density (BMD) and described the trabecular bone volume fraction as a surrogate for bone mineral density.

Goodsitt *et al* (2014) evaluated the use of dual-energy quantitative computed tomography (DEQCT) to determine the spatial distribution of bone marrow for dosimetry in molecular radiotherapy. They demonstrated that DEQCT is a promising technique to estimate the spatial volume fraction of red marrow and trabecular bone.

Recently, Booz *et al* (2017) evaluated an algorithm based on DEQCT imaging to assess BMD in the lumbar spine and compared the results with x-ray absorptiometry (DEXA). They conclude that the quantification of BMD in lumbar vertebrae using DECT is feasible.

The implementation and validation of a methodology that permits the quantification of the bone volume fraction in spongiosa (trabecular bone plus its supported soft tissue (ICRP 2002)) in patients undergoing molecular radiotherapy is a necessity to study the impact of the spatial distribution of fat (yellow marrow), hematopoietic tissue (red marrow) and trabecular bone in the bone marrow on the absorbed dose to each tissue, with special interest in the red marrow absorbed dose. The aim of this study is to validate a phantomless method for applying DEQCT to quantify the trabecular bone volume fraction (or bone volume fraction in spongiosa) for bone marrow dosimetry in molecular radiotherapy particularly with equipment that is readily available in a nuclear medicine department.

Methods

CT images were acquired with a dual-source CT (DSCT) (SOMATOM Force, Siemens Healthineers 2018) and with the CT part of a SPECT/CT hybrid system (Symbia Intevo Bold, Siemens Healthineers 2018) with adaptable CT voltage (80, 110, and 130 kV). Dual energy x-ray absorptiometry (DEXA) was performed with a Lunar Prodigy Advance DEXA system (GE Healthcare).

Analysis of the calibration phantom CT images was performed in Fiji (version ImageJ 1.51 g) (Schindelin *et al* 2012, Schneider *et al* 2012), while the CT images of the patient, the Model 062M electron density phantom (computerized imaging reference systems, CIRS) and the European Spine Phantom (Kalender 1992) were analyzed using the Segment Editor tool of 3D Slicer (version 4.8.1) (Fedorov *et al* 2012, Kikinis *et al* 2014). All mathematical calculations were performed in R (version 3.5.1) (R Core Team 2008).

Fabrication of a validation phantom (homemade phantom)
To validate the material composition quantification techniques applied in this study, 50 ml vials with different compositions of fat, water, and hydroxyapatite were prepared:

- A first set was developed for validating the hydroxyapatite quantification. It consisted of three 50 ml vials with different hydroxyapatite concentrations. Each sample was composed of a mixture of 50% water and 50% Poly(2-hydroxyethyl methacrylate) (pHEMA) mixed with a different concentration of hydroxyapatite ($100\,\mathrm{mg\,cm^{-3}}$, $200\,\mathrm{mg\,cm^{-3}}$, $300\,\mathrm{mg\,cm^{-3}}$) from *in situ* hydrolysis of alpha-tricalcium phosphate (α-TCP) in the water-pHEMA mixture as described by Christel *et al* (2013) for the fabrication of dual setting calcium phosphate bone cements. Considering a hydroxyapatite density of $3000\,\mathrm{mg\,cm^{-3}}$, the volume fraction of hydroxyapatite in each sample corresponded to 0.033, 0.067 and 0.10, respectively. α-TCP was synthesized from a 2:1 molar mixture of dicalcium phosphate anhydrous ($CaHPO_4$) and calcium carbonate ($CaCO_3$) by sintering the powder mixture at 1400 °C for 5 h in a high temperature furnance (Oyten), followed by quenching to room temperature. The sintering cake was manually crushed and then ball milled for 4 h in a planetary ball mill (PM400, Retsch GmbH).
- A second set was developed to evaluate the capability of CT-based hydroxyapatite quantification in a fat-water medium. This set was composed of two samples from the same preparation: each sample consisted of a mixture of 50% agar (based on Hines *et al* (2009)) and 50% paraffin (viscous) mixed with a $150\,\mathrm{mg\,cm^{-3}}$ concentration of hydroxyapatite (calcium phosphate tribasic, Thermo Fisher GmbH), corresponding to a 0.05 hydroxyapatite, 0.475 fat, and 0.475 water volume fraction in both vials. In comparison to Hines *et al* (2009), the preparation differed in the following points: (1) we used paraffin instead of peanut oil. (2) We did not use gadolinium or iron because the use of these elements is related simulation of liver tissue in studies with MRI.
- Finally, a third set of three more 50 ml vials was prepared: (1) distilled water, (2) pure paraffin, and (3) pure agar.

All vials were located in a water-filled NEMA phantom to simulate soft tissue attenuation. They were mounted in the phantom by a 3D-printed insert. The sample arrangement is shown in figure 1.

Image of phantoms acquired with DSCT
Two set of images following the clinical protocol for multiple myeloma were acquired, the acquisition parameter are specified in table 1. In the dual-source CT, the low and high energy images were acquired simultaneously. Each set of images was reconstructed with default kernels (Qr40 and Br59) based on the clinical protocol for multiple myeloma.

Image of phantoms acquired with SPECT/CT
One set of CT images was acquired using an abdominal imaging protocol, the acquisition parameter are specified in table 1. Both image volumes were acquired subsequently and they were reconstructed using the I41s kernel.

DEQCT—mass fraction method: three material decomposition based on spectral x-ray attenuation method
In our study, we used the methodology proposed by Liu *et al* (2009). This methodology makes use of the x-ray tube spectrum and the detector sensitivity. For the SPECT/CT, the manufacturer provided information related to x-ray filter arrangement and bowtie filter attenuation profiles. Based on this information, the x-ray tube spectra were created using the Siemens online tool for the simulation of x-ray spectra (Simens Healthineers 2018). For the DSCT, the manufacturing company provided the isocenter x-ray tube spectra for 80 kV, 120 kV, 150 kV and 150 kV with Sn filter. Due to the lack of a 90 kV spectrum, this spectrum was generated by choosing the filter arrangement (titanium and aluminum) that reproduced the 80 kV and 120 kV spectra with the lowest difference. For both systems, the detector sensitivity was extracted from Liu *et al* (2009) under the assumption of GdOS scintillators.

Lastly, the quantification method presented by Liu *et al* (2009) requires the mass attenuation coefficients of (i) the elements with atomic number between 1 and 30, and (ii) the materials to be quantified in the respective energy range of the x-ray tube spectrum. The materials to be quantified were: (i) Patient tissues: soft tissue, adipose tissue and cortical bone, material definition from Report 44 of the International Commission on Radiation Units and Measurements (ICRU) (White 1989). (ii) Phantom samples composition was simplified to: water, adipose tissue and hydroxyapatite, the element weight fractions for water and hydroxyapatite are specified in the supplementary material table 1 (stacks.iop.org/PMB/64/205014/mmedia). The attenuation coefficient data was taken from the program XMuDat (version 1.0.1) (International Atomic Energy Agency NDSV 1998).

Following the methodology proposed by Heismann *et al* (2003) and Liu *et al* (2009), a lookup table for each x-ray tube spectrum and the detector sensitivity arrangement was prepared. This lookup table provides effective density ($\rho_{\mathrm{eff,lookup\text{-}table}}$) and effective atomic number (Z_{eff}) of the material to be quantified.

Next, the mass fractions (*MF*) can be obtained by solving the following equation system (Liu *et al* 2009):
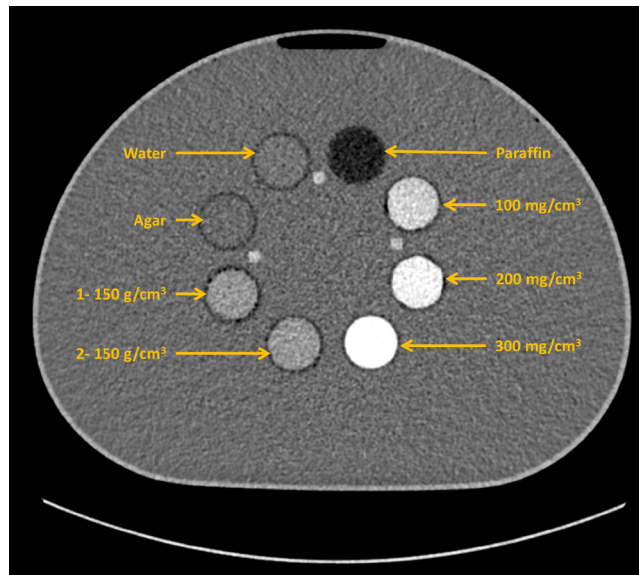
Figure 1. Axial view of set of calibration and quantification samples. Equipment: somaton force. Reconstruction kernel: Qr40, energy: 80 kV.

Table 1. Acquisition parameter for DSCT and SPECT/CT.

CT System	Image	Voltage (kV)	Tube Current-Exposure Time Product (mAs)	Collimation (mm)	Pitch	Slice thickness (mm)	CTDI$_{\text{vol}}$ (mGy)
DSCT	1	80	158	64 × 0.6	0.6	1	3.23
		150	90				2.79
	2	90	130	64 × 0.6	0.6	1	4
		150	90				2.82
SPECT/CT	1	80	70	16 × 0.6	0.6	1	2.39
		130	53				6.39

$$\mu_{\text{eff},E_1} = C \cdot K \cdot \rho_{\text{eff,lookup-table}} \int_{E=\ 0\,\text{keV}}^{E\ =E_1} w_{E_1}(E) \left[MF_1 \times \mu_{m,E_1,1}(E) + MF_2 \times \mu_{m,E_1,2}(E) + (1 - MF_1 - MF_2) \times \mu_{m,E_1,3}(E) \right] dE \tag{2}$$

$$\mu_{\text{eff},E_2} = C \cdot K \cdot \rho_{\text{eff,lookup-table}} \int_{E=\ 0\,\text{keV}}^{E\ =E_2} w_{E_2}(E) \left[MF_1 \times \mu_{m,E_2,1}(E) + MF_2 \times \mu_{m,E_2,2}(E) + (1 - MF_1 - MF_2) \times \mu_{m,E_2,3}(E) \right] dE \tag{3}$$

$$1 = MF_1 + MF_2 + MF_3. \tag{4}$$

E_1 and E_2 correspond to the two energies used for image acquisition. MF_1, MF_2 and MF_3 are the mass fractions of the quantified materials (e.g. hydroxyapatite, fat or adipose tissue, and water or soft tissue). μ_{eff} is the effective attenuation coefficient in a volume-of-interest (VOI). $\mu_{m,E_{1,2},1}$, $\mu_{m,E_{1,2},2}$ and $\mu_{m,E_{1,2},3}$ are the effective mass attenuation coefficients of the quantified materials (Heismann *et al* 2003, Liu *et al* 2009). They were calculated for each x-ray beam spectrum and for: water, hydroxyapatite, soft tissue, adipose tissue and cortical bone. These materials were used as decomposition materials. C is an empirical correction factor documented by Liu *et al* (2009) and Azevedo *et al* (2016) to correct the effective density ($\rho_{\text{eff,lookup-table}}$) obtained from the lookup table due to the increase of the effective atomic number in the VOI. A second constant K was used in the calculation process to correct the effective density ($\rho_{\text{eff,lookup-table}}$) obtained from the lookup table. The constant K corrects the lack of specific information of the x-ray tube spectrum or detector sensitivity function. Both constants (C and K) permit to calculate the effective density ($\rho_{\text{eff}} = C \times K \times \rho_{\text{eff,lookup-table}}$) in the VOI. An example of C and K determination can be found in the supplementary material as an appendix. $w_{E_{1,2}}$ is a weighting function for E_1 and E_2, which is defined as $w_{E_{1,2}} = S(E) D(E) / \int_{E=\ 0\,\text{keV}}^{E=E_{1,2}} S(E) D(E) dE$, where $S(E)$ is the x-ray tube spectrum and $D(E)$ is the detector sensitivity function.

The main goal of this study is to quantify the trabecular bone volume fraction. Therefore all hydroxyapatite mass fraction (MF_{HA}) values were converted into hydroxyapatite volume fraction (VF_{HA}) using equation (5).

$$\mathrm{VF_{HA}} = \frac{\rho_{\mathrm{eff}} \times \mathrm{MF_{HA}}}{\rho_{\mathrm{HA}}}. \tag{5}$$

ρ_{HA} corresponds to hydroxyapatite density.

Analysis of validation phantom

The mass fraction method was applied to all phantoms. The hydroxyapatite volume fraction in the pHEMA-Water (50/50) samples was quantified to correlate the measured hydroxyapatite volume fraction of each CT image set ($\mathrm{VF_{HA\_DSCT}}$ and $\mathrm{VF_{HA\_SPECT/CT}}$) against the theoretical hydroxyapatite volume fraction ($\mathrm{VF_{HA\_0}}$). For the first set of samples, the three-unknown equation system (equations (2)–(4)) was solved by setting the fat fraction to zero in equation (4). Hydroxyapatite, water and fat fraction were quantified in the second set of samples (150 mg cm^{-3} hydroxyapatite) presuming hydroxyapatite, water and adipose tissue as material composition, this approach is applied in all measurement performed on phantoms. An average value was calculated from both samples. All results are displayed as Bland-Altman plots.

Quantification of bone mineral content in the European spine phantom using DEXA, DSCT and SPECT/CT

The European Spine Phantom (ESP) consists of three vertebrae, each one with three compartments: (i) spongiosa, (ii) wall and endplate, and (iii) arch and processes. The bone mineral content (BMC) of each vertebra (1 to 3) of the ESP ($\mathrm{BMC_{ESP}}$) are 4.5 g hydroxyapatite (HA), 9.0 g of HA and 13.5 g of HA (Kalender 1992).

Using DEXA, ten measurements of the bone mineral area density ($\mathrm{BMD_{DEXA}}$) of ESP (Kalender 1992) were performed in anterior-posterior position. Next, the area of the automatically selected DEXA-ROI was quantified. Subsequently, the $\mathrm{BMC_{DEXA}}$ was quantified by multiplication of $\mathrm{BMD_{DEXA}}$ by the DEXA-ROI area. Afterwards, CT imaging of the ESP (Kalender 1992) was performed using the DSCT and the SPECT/CT systems. The mean CT# (HU) for each whole vertebra excluding the transverse process was obtained in a VOI analysis. The transverse processes were excluded because they are suppressed from the quantification region by the automatic threshold segmentation of the DEXA workflow. For quantification, the mass fraction method was applied. Subsequently, the $\mathrm{BMC_{DSCT}}$ (or $\mathrm{BMC_{SPECT/CT}}$) was obtained by multiplication of hydroxyapatite volume fraction with the nominal hydroxyapatite density (3000 mg cm^{-3}) to obtain $\mathrm{BMD_{DSCT}}$ (or $\mathrm{BMD_{SPECT/CT}}$). Then, $\mathrm{BMD_{DSCT}}$ was multiplied by the volume of the VOI to obtain $\mathrm{BMC_{DSCT}}$. In addition, the relative errors between each imaging modality ($\mathrm{BMC_{DEXA}}$, $\mathrm{BMC_{DSCT}}$ or $\mathrm{BMC_{SPECT/CT}}$) and $\mathrm{BMC_{ESP}}$ were quantified. All results are displayed as Bland-Altman plots.

Quantification of bone mineral density in spongiosa regions of European spine phantom using DSCT and SPECT/CT

ESP nominal values of bone mineral density ($\mathrm{BMD_{ESP}}$) for spongiosa in vertebrae 1, 2 and 3 are 50 mg cm^{-3} of hydroxyapatite (HA), 100 mg cm^{-3} of HA and 200 mg cm^{-3} of HA (Kalender 1992). Using DSCT and SPECT/CT, the mean CT# (HU) for the spongiosa region of each vertebra was measured. The BMD of the spongiosa regions were measured by multiplication of hydroxyapatite volume fraction with the nominal hydroxyapatite density (3000 mg cm^{-3}). The relative errors between $\mathrm{BMD_{ESP}}$ and the bone mineral density measured based on each CT image set ($\mathrm{BMD_{DSCT}}$ and $\mathrm{BMD_{SPECT/CT}}$) were calculated.

Clinical application of mass fraction method in a patient image set

To show that the method can be applied clinically, a patient that had previously undergone DEXA and DSCT imaging in our institution was retrospectively selected. The time difference between the DEXA and the DSCT study was 1 week. The related DEXA study of that patient had quantified the $\mathrm{BMD_{DEXA}}$ of lumbar vertebrae 1 to 4. The patient was scanned for acute pulmonary embolism using DSCT. The DSCT study contains an imaging volume covering the thorax, including complete lumbar vertebrae 1 and 2. Acquisition parameters were 90 kV/150 kV (with Sn filter), 120/63 mAs exposure, with 96 × 0.6 mm collimation, slice thickness 1.5 mm, 0.55 pitch, and a Qr40 reconstruction kernel. The CTDI$_{\mathrm{vol}}$ was 3.50/1.85 mGy. Figure 2 shows the segmentation of lumbar vertebrae 1 and 2, in which transverse processes were not included.

Next, the mass fraction method was applied to the patient images using hydroxyapatite, soft tissue and adipose tissue as material composition. The hydroxyapatite mass fraction, hydroxyapatite volume fraction and bone mineral content were quantified in each vertebra (again excluding the transverse processes). Also, hydroxyapatite mass fraction and hydroxyapatite volume fraction were quantified in spongiosa regions.

Methods to quantify the bone volume fraction

In this study two methods were used to quantify the bone volume fraction: (i) to use a reference ratio of mineral bone mass fraction to total bone mass fraction ($R_{\mathrm{HA/B}}$) and (ii) to change from hydroxyapatite chemical
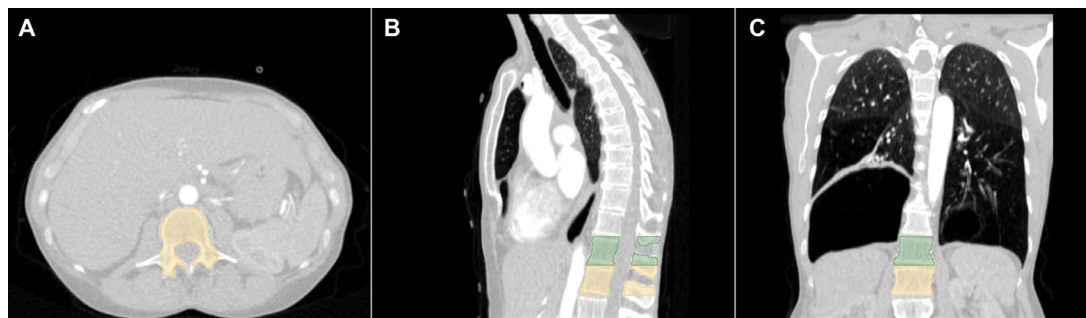
Figure 2. CT segmentation of lumbar vertebrae 1 and 2. (A) Axial, (B) sagittal and (C) coronal view. Reconstruction kernel: Qr40, energy: 150 kV (using Sn filter).

description to cortical bone chemical description (ICRU report 44 (White 1989)) in the material definition used in the mass fraction method.

- *First method: Reference Ratio of Mineral Bone Mass Fraction to Total Bone Mass Fractions*

Considering that bone is composed of minerals and an organic matrix, the mass fraction method (by using DEQCT) provide directly the hydroxyapatite mass fraction (MF_{HA}). This parameter is related with the total bone mass fraction by the ratio of mineral bone mass fraction to total bone mass fraction ($R_{HA/B} = MF_{HA}/MF_B$). Therefore the bone volume fraction (VF_B) can be defined as:

$$VF_B = \frac{\rho_{eff} \times MF_B}{\rho_B} = \frac{\rho_{eff}}{\rho_B} \frac{MF_{HA}}{R_{HA/B}}. \tag{6}$$

ρ_B is the cortical bone density ($1.92\,\text{g cm}^{-3}$) (White 1989).

The $R_{HA/B}$ can be quantified by measuring the relative amount of mineral and organic material in bone samples. Quelch *et al* (1983) quantified the percentages by mass of minerals and organic material in dry, fat-free human vertebra. They documented a percentage value of mineral bone equal to 66.3% (adult vertebra). This value is used as reference value for $R_{HA/B}$ (0.663). Then the equation (6) can be re-expressed as:

$$VF_B = \frac{\rho_{eff}}{\rho_B} \frac{MF_{HA}}{0.663} \tag{7}$$

- *Second Method: Change the Chemical Description from Hydroxyapatite to Cortical Bone*

The mass fraction method is based on the element composition of the materials to be quantified. This provides flexibility for quantifying other materials. Since trabecular bone has the same elemental composition as cortical bone (Woodard and White 1982), it is possible to change from hydroxyapatite quantification to bone quantification (using cortical bone element composition from ICRU report 44 (White 1989)).

Both methods to quantify the bone volume fraction were applied to the patient data set. Therefore, the bone mass fraction and the bone volume fraction were quantified in each vertebra (excluding the transverse processes) and in the spongiosa region. Lastly, the ratio of mineral bone mass fraction to total bone mass fraction ($R_{HA/B} = MF_{HA}/MF_B$) was calculated.

Results

The hydroxyapatite volume fraction was quantified for both CT systems (DSCT and SPECT/CT). In case of the DSCT, hydroxyapatite volume fraction was quantified for two image reconstruction kernels (Qr40 and Br59) and for two different dual-energy settings (80/150 kV and 90/150 kV). Therefore, four different parameter sets were used to quantify the hydroxyapatite volume fraction with the DSCT: Br59–80/150 kV, Qr40–80/150 kV, Br59–90/150 kV and Qr40–90/150 kV. For the SPECT/CT, only one combination of image reconstruction kernel (I41s) and dual-energy setting (80/130 kV) was used to create the image I41s-80/130 kV. Results for these five images are presented in the next sections related to hydroxyapatite volume fraction quantification in the phantoms.

Quantification of hydroxyapatite volume fraction in the validation phantom

Figure 3 shows Bland-Altman plots and relative errors of the hydroxyapatite volume fraction quantification of the samples located in the validation phantom. Bland-Altman analysis revealed good agreement between
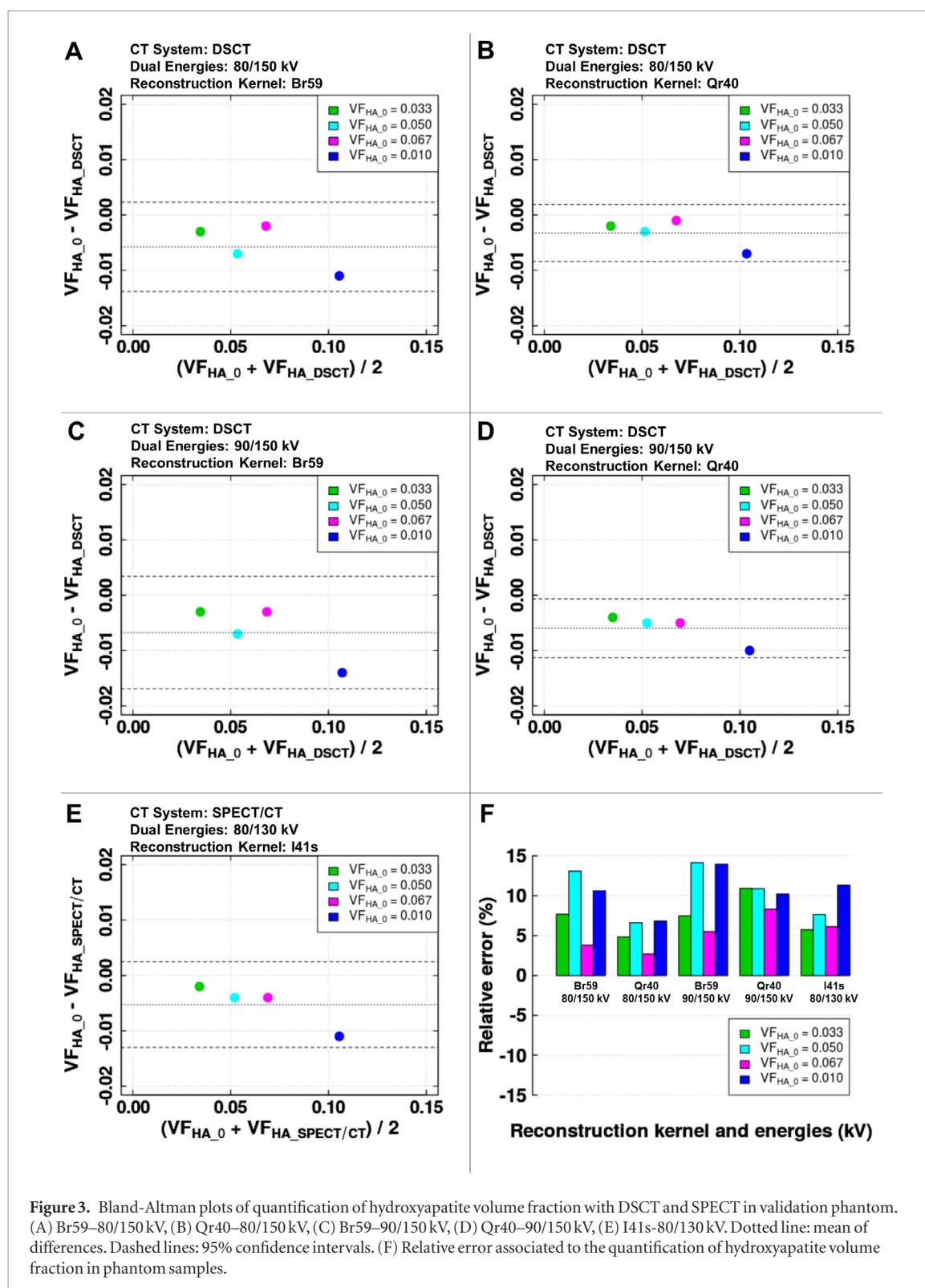
Figure 3. Bland-Altman plots of quantification of hydroxyapatite volume fraction with DSCT and SPECT in validation phantom. (A) Br59–80/150 kV, (B) Qr40–80/150 kV, (C) Br59–90/150 kV, (D) Qr40–90/150 kV, (E) I41s-80/130 kV. Dotted line: mean of differences. Dashed lines: 95% confidence intervals. (F) Relative error associated to the quantification of hydroxyapatite volume fraction in phantom samples.

the quantified hydroxyapatite volume fraction of each CT image set (VF_{HA_DSCT} and $VF_{HA\_SPECT/CT}$) and the theoretical hydroxyapatite volume fraction (VF_{HA_0}). In addition, for each image-based quantification, the bias and limits of the confidence intervals for each Bland-Altman plot are presented in table 2. All plots show a negative bias, which indicates that the quantification method overestimates the hydroxyapatite volume fraction. The maximum relative error was 14.2% for sample 150 mg cm^{-3} HA in image Br59–90/150 kV.

Effective density (ρ_{eff}) and effective atomic number (Z_{eff}) of the samples located in the validation phantom are listed in supplementary table 2. The quantification of SPECT/CT image showed a better agreement of ρ_{eff} and Z_{eff} with their nominal values. Therefore, a better material description was achieved by the SPECT/CT.

Table 2. Data from Bland-Altman analysis of the quantification of hydroxyapatite volume fraction in the validation phantom.

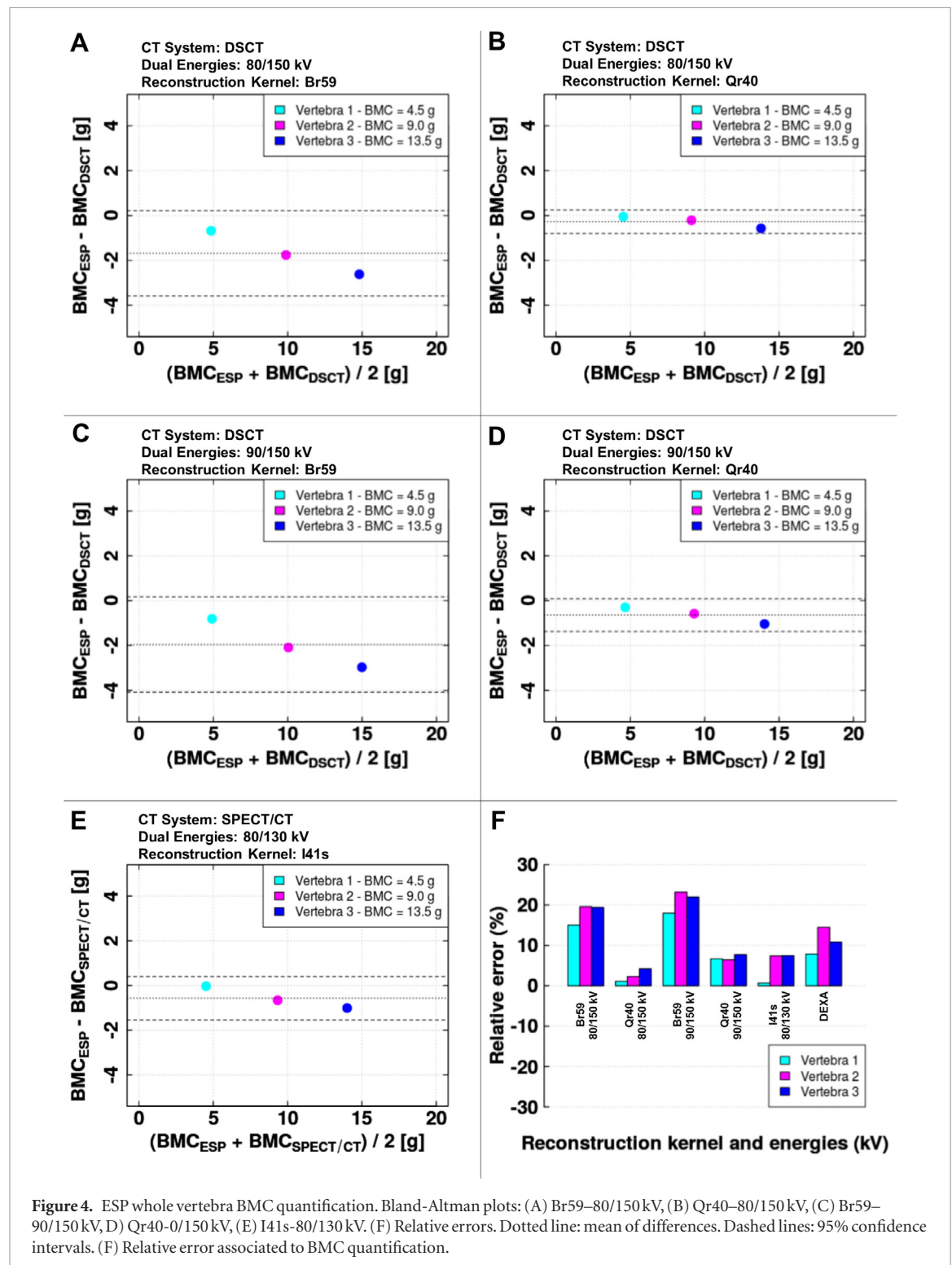| CT system	Dual energy (kV)	Reconstruction kernel	Bias (VF$_{HA}$)	Lower limit (VF$_{HA}$)	Upper limit (VF$_{HA}$)
SPECT/CT	80/130	I41s	−0.005	−0.013	0.003
DSCT	80/150	Qr40	−0.003	−0.008	0.002
		Br59	−0.006	−0.014	0.002
	90/150	Qr40	−0.006	−0.011	−0.001
		Br59	−0.007	−0.017	0.003

VF$_{HA}$: hydroxyapatite volume fraction.

Figure 4. ESP whole vertebra BMC quantification. Bland-Altman plots: (A) Br59–80/150 kV, (B) Qr40–80/150 kV, (C) Br59–90/150 kV, D) Qr40-0/150 kV, (E) I41s-80/130 kV. (F) Relative errors. Dotted line: mean of differences. Dashed lines: 95% confidence intervals. (F) Relative error associated to BMC quantification.

Table 3. Data from Bland-Altman analysis of the quantification of bone mineral content (whole vertebra) in the European Spine Phantom.

CT system	Dual energy (kV)	Reconstruction kernel	Bias (g HA)	Lower limit (g HA)	Upper limit (g HA)
SPECT/CT	80/130	I41s	−0.567	−1.540	0.407
DSCT	80/150	Qr40	−0.277	−0.799	0.245
		Br59	−1.687	−3.592	0.219
	90/150	Qr40	−0.640	−1.372	0.092
		Br59	−1.956	−4.085	0.172

HA: hydroxyapatite.

Figure 5. ESP spongiosa region BMD quantification. Bland-Altman plots: (A) Br59–80/150 kV, (B) Qr40–80/150 kV, (C) Br59–90/150 kV, (D) Qr40–90/150 kV, (E) I41s-80/130 kV. (F) Relative errors. Dotted line: mean of differences. Dashed lines: 95% confidence intervals. F) Relative error associated to BMD quantification.
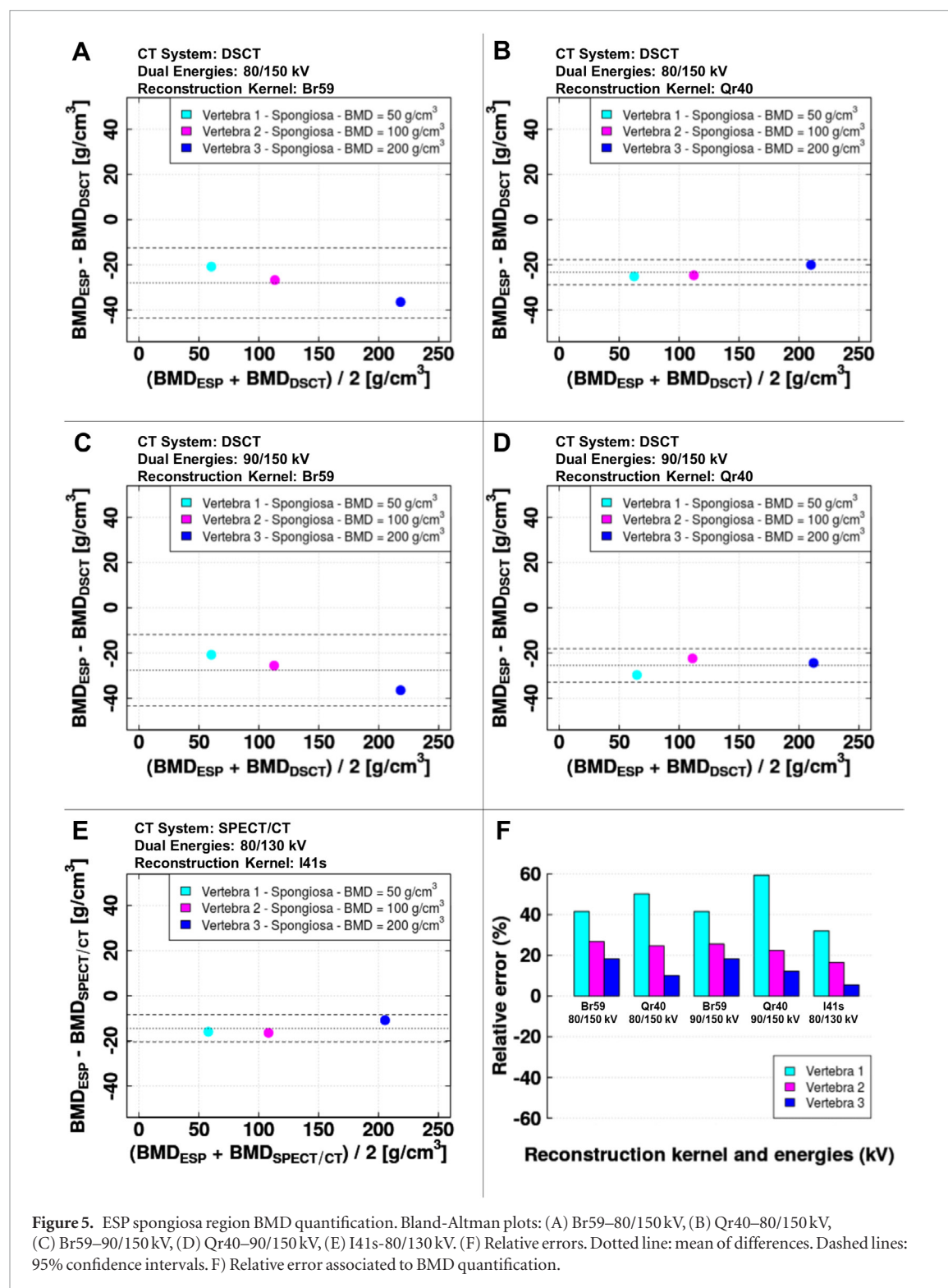
Table 4. Data from Bland-Altman analysis of the quantification of bone mineral density in spongiosa region of the European Spine Phantom.

CT system	Dual energy	Reconstruction kernel	Bias (mg/cm^3 HA)	Lower limit (mg/cm^3 HA)	Upper limit (mg/cm^3 HA)
SPECT/CT	80/130	I41s	−14.433	−20.499	−8.367
DSCT	80/150	Qr40	−23.240	−28.758	−17.722
		Br59	−29.963	−43.457	−12.470
	90/150	Qr40	−25.473	−32.887	−18.060
		Br59	−27.573	−43.349	−11.797

HA: hydroxyapatite.

Table 5. Values of mass and volume fractions of HA and bone in lumbar vertebrae 1 and 2 from a patient image set.

Region		Parameter					
		MF$_{HA}$	VF$_{HA}$	MF$_B$	VF$_B$[b]	VF$_B$[c]	R$_{HA/B}$
Whole Vertebra[a]	Lumbar Vertebra 1	0.138	0.052	0.124	0.249	0.148	0.554
	Lumbar Vertebra 2	0.145	0.056	0.132	0.261	0.157	0.556
Spongiosa	Lumbar Vertebra 1	0.113	0.039	0.093	0.203	0.071	0.557
	Lumbar Vertebra 2	0.116	0.040	0.095	0.208	0.072	0.558

MF$_{HA}$: hydroxyapatite mass fraction, VF$_{HA}$: hydroxyapatite volume fraction, MF$_B$: bone mass fraction, VF$_B$: bone volume fraction.
[a] Excluding transverse processes.
[b] First volume fraction calculation method.
[c] Second volume fraction calculation method.

Quantification of fat, water and HA in the validation phantom

Decomposition of the three materials fat, water and hydroxyapatite was not possible as the values of $\mu_{m,Fat}$ and $\mu_{m,Water}$ are too similar. Therefore, in our study, the determinant of the coefficient matrix (equation A3 in Liu *et al* (2009)) resulted in a number close to zero.

Quantification of bone mineral content in European spine phantom

Figure 4 shows the Bland-Altman plots and relative errors of the quantification of BMC in each vertebra of ESP using the mass fraction method. The BMC measured by DEXA was 4.9 ± 0.3 g of hydroxyapatite (HA), 10.3 ± 0.3 g of HA, and 15.0 ± 0.3 g of HA for vertebrae 1, 2 and 3 of the ESP, respectively (mean $\pm$ standard deviation over 10 measurements). The relative errors for DEXA lay between 14.5% and 7.9%. Lower errors and better agreement between measured values (BMC$_{DSCT}$ or BMC$_{SPECT/CT}$) and nominal values (BMC$_{ESP}$) were achieved based on the Qr40 (DSCT) and the I41s (SPECT/CT) based quantification.

For each image-based quantification, the bias and the confidence interval for each Bland-Altman plot are presented in table 3. All plots show a negative bias, which indicates that the quantification method overestimates the BMC. The Br59 (DSCT) based quantification showed the largest standard deviations.

Effective density and effective atomic number for ESP are listed in supplementary table 3. Although there are no nominal values to compare, they are reported for future comparison studies.

Quantification of bone mineral density in spongiosa regions of European spine phantom

Figure 5 shows Bland-Altman plots and relative error of the quantification of BMD$_{DSCT}$ (or BMD$_{SPECT/CT}$) in the spongiosa region for each vertebra of the ESP. For each image-based quantification, the bias and limits of the confidence interval for each Bland-Altman plot are presented in table 4. All plots show a negative bias, which indicates that the quantification method overestimates the bone mineral density in the spongiosa region. The best agreement between the measured values and the nominal values was obtained with the I41s (SPECT/CT) based quantification.

The quantification of images acquired with the 80/150 kV dual energy setting showed errors between 10.0% and 50.2% for Qr40 and between 18.2% and 41.5% for Br59. The quantification of images acquired with 90/150 kV showed relative errors between 12.2% and 59.4% for Qr40 and between 18.2% and 41.5% for Br59. Quantification based on SPECT/CT showed the lowest relative errors ranging from 5.4% to 32.0%.

Clinical application of mass fraction method in a patient image set

The patient image set analyzed in this study corresponds to a 49.5 years old female patient with a diagnosis of osteopenia at the border to osteoporosis (DEXA T-score of -3.6 and 3.0 in lumbar vertebrae 1 and 2, respectively). The BMC values quantified by DEXA were 8.0 g and 10.9 g for lumbar vertebrae 1 and 2, respectively. The relative errors between DEXA and DSCT were 7.6% and -8.4% for lumbar vertebra 1 and 2, respectively.

The bone volume fraction obtained by using the first calculation method (reference ratio of mineral bone to total bone mass fractions) are presented in table 5, together with the bone volume fraction obtained by using the second method (change the chemical description from hydroxyapatite to cortical bone). Also the mass fractions of hydroxyapatite and bone the volume fractions of hydroxyapatite and bone, and the ratio of mineral bone mass fraction and total bone mass fraction ($R_{HA/B} = MF_{HA}/MF_B$) are included in table 5.

Discussion

In this study, we propose a method which allows to quantify the mass and volume fraction of bone using DEQCT.

Quantification of VF_{HA} in the validation phantom

In the first part of this study, the mass fraction method was tested in the lower regime of hydroxyapatite concentrations (between 100 mg cm^{-3} and 300 mg cm^{-3} HA). Thomsen *et al* (2015) quantified the mineralized bone volume per total volume (BV/TV) in lumbar vertebra L2 of 41 women and 39 men by evaluating the 3D microstructure using micro-CT (μCT). They documented a linear correlation between trabecular BV/TV and age in women ($r = -0.83, p = 2.0 \times 10^{-11}$) and men ($r = -0.74, p = 8.8 \times 10^{-8}$). This correlation showed that trabecular BV/TV decreased significantly with age in women and men. Using the linear regression parameters proposed by Thomsen *et al* (2015), it is possible to quantify the BV/TV for different ages. For a 20, 50 and 80 year old male, the trabecular BV/TV were 0.08, 0.12, and 0.15. In case of a female, these values were 0.07, 0.11, and 0.15. The hydroxyapatite volume fraction and the BV/TV are equivalent definitions. In this study, hydroxyapatite volume fractions of the samples in the validation phantom were 0.033, 0.067 and 0.10. These hydroxyapatite volume fractions were selected because: (i) they are representative for the patient age group that can be candidate for a molecular radiotherapy treatment and (ii) they are in the range of values in which is expected the greatest quantification errors (Emami *et al* 2011). For other bone sites with a larger bone density such as femur neck, iliac crest or cranium, DEQCT must be additionally/further evaluated with representative hydroxyapatite concentrations.

The mass fraction method provides a phantom-independent methodology as it is based on mass fraction conservation. However, it requires a good characterization of the x-ray beam and detector.

In this study, conservation of volume fraction was assumed. Liu *et al* (2009) explained that this assumption of a constant volume does not always hold. As an example, for solutions in which the solute dissolves in the solvent, the solute will take a smaller portion of the solution's volume. In our study, however, the conservation of volume fraction assumption holds as hydroxyapatite, fat and water are immiscible materials.

Furthermore, the use of hydroxyapatite in solutions or in polymers (as in our study) is a standard in CT experiments related with bone quantification (Goodsitt *et al* 1991, Kalender 1992, Liu *et al* 2009, Goodsitt *et al* 2014). The main limitation in working with hydroxyapatite is the formation of clusters when it interacts with a solvent. The technique applied in our study was documented by Christel *et al* (2013). The size of α-TCP particles is approximately 9.34 μm, and they are distributed homogeneously in the medium. Thomsen *et al* (2015) measured the trabecular bone thickness in lumbar vertebra 2. Using the linear regression parameters proposed by Thomsen *et al* (2015), it is possible to calculate the expected trabecular bone thickness for a 20, 50 and 80 year old male: 139.5 μm, 137.13 μm, and 134.8 μm, respectively. Also, for a 20, 50 and 80 year old female: 123.3 μm, 126.65 μm, and 130.04 μm, respectively. Considering the volume of a CT voxel (larger than 1 mm^3), it is expected that the hydroxyapatite spatial distribution achieves a good representation of the trabecular bone spatial distribution.

The Bland-Altman plots from figures 3(a)–(e) show that for all image-based quantification, the mass fraction method overestimates the hydroxyapatite volume fraction. This observation becomes clearer in figure 3(f) where all relative errors are positive and below 15%. A possible source of error is the disagreement between the real chemical composition of the materials in the phantom sample and the chemical composition used in the mass fraction method. To quantify the samples in the validation phantom, we used hydroxyapatite, adipose tissue and water as material definition, although the samples were made of a mix of pHEMA-water, agar, paraffin and hydroxyapatite. A second error source lies in the two empirical corrections applied to obtain the effective density. These corrections were obtained from the hydroxyapatite quantification in a reference bone sample of the phantom CIRS Model 062M. Therefore, these corrections are dependent on the chemical composition of the reference bone sample of the phantom CIRS Model 062M.

The quantification of the $150\,\mathrm{mg\,cm^{-3}}$ hydroxyapatite samples in an inhomogeneous medium (47.5% volume of fat and 47.5% volume of agar) shows a similar agreement between the nominal value of hydroxyapatite volume fraction (HA_{VF_0}) and the hydroxyapatite volume fraction quantified with each CT system (HA_{VF_DSCT} and $HA_{VF\_SPECT/CT}$) as the pHEMA-water and hydroxyapatite samples. Although fat quantification was not possible in this study, it is possible to observe that the inclusion of fat in the sample (as it is present throughout the human body) and the assumption of a fat fraction equal to zero in the equation system (equation (4)) will not affect the hydroxyapatite quantification using the mass fraction method.

Quantification of bone mineral content in European spine phantom (ESP)

The ESP provides a realistic geometry in which the use of different concentrations of hydroxyapatite in each compartment (i) spongiosa, (ii) wall and endplate and (iii) arch and processes) and changes in compartment size enables the simulation of different geometries and beam hardening.

DEXA is the clinical gold standard for BMD quantification. In this study, DEXA and DEQCT were compared by quantifying BMC. Figure 4 shows that the quantification of BMC in whole vertebra is feasible using the mass fraction method. The Qr40 based quantification agree well with the BMC_{ESP} nominal values (figures 4(b) and (d)), the I41s based quantification presenting a similar tendency. Also, the Qr40 and I41 based quantifications show a lower bias and a narrower interval of confidence than the Br59 based quantification. Therefore, they provide a more accurate measurement of the BMC in the whole vertebra. For all image-based quantification, the mean difference decreases with the increase of BMC (see Bland-Altman plots). This tendency is even more visible in the Br59 based quantification. The Br59 images enhance the bone signal, which might be the reason of the large relative error obtained from their quantification (figure 4(f)).

Comparing DEXA with DEQCT (figure 4(f)), one can see that for the Qr40 and I41s based quantification, the relative errors between two quantification modalities are similar.

Quantification of bone mineral density in spongiosa regions of European spine phantom

The main goal of this study was the quantification of bone volume fraction in the bone marrow for dosimetry in molecular radiotherapy. The spongiosa region of ESP provides an optimal geometrical configuration to validate the mass fraction method.

For the ESP dimensions (25 cm lateral and 18 cm anterior-posterior), quantification on images acquired with SPECT/CT provide the lowest relatives errors of 32.0% for $50\,\mathrm{mg\,cm^{-3}}$ HA, 16.5% for $100\,\mathrm{mg\,cm^{-3}}$ HA and 5.4% for $200\,\mathrm{mg\,cm^{-3}}$ HA. Liu *et al* (2009), for the same hydroxyapatite concentrations but in a cylindrical geometry, documented relative errors of -20%, -11% and -18% in the mass fraction of hydroxyapatite using a second generation DSCT (SOMATOM Definition DS, Siemens Healthineers 2018). The difference in geometry between the samples (cylinders versus vertebrae) might play an important role, due to the beam hardening caused by the cortical wall of the vertebral bodies, the spinous process and the transverse processes over the spongiosa region. Additionally, the decrease of the relative error in SPECT/CT-based quantification with increasing hydroxyapatite concentrations in the ESP vertebrae can be related to the chemical description of the reference materials (water, adipose tissue and hydroxyapatite). ESP vertebrae are composed of a mix of HA and epoxy-resin. Therefore, with the increase of hydroxyapatite concentration, the difference between water and epoxy-resin becomes less important.

The hydroxyapatite volume fraction of the spongiosa region of the first vertebra of the ESP ($50\,\mathrm{mg\,cm^{-3}}$ hydroxyapatite—0.0167 hydroxyapatite volume fraction) is a value that is out of the calculated range of hydroxyapatite volume fraction obtained from Thomsen *et al* (2015) (between 0.08 and 0.15 for men and between 0.07 and 0.15 for women). By using the SPECT/CT for hydroxyapatite volume fraction quantification, the maximum expected error is similar to the one obtained in vertebra 3 of the ESP ($200\,\mathrm{mg\,cm^{-3}}$ hydroxyapatite—0.067 hydroxyapatite volume fraction), which was 5.44%. In case of DSCT, the expected error is below 10% (80/150 kV) and 13% (90/150 kV) by using Qr40 based quantification. In patients with malignant bone lesion in vertebrae is expected lower bone mineral density (or hydroxyapatite volume fraction) due to the bone destruction (osteolytic lesions) or a buildup of new weaker bone (osteoblastic lesion) (Lipton *et al* 2009). Therefore, the quantification of hydroxyapatite volume fraction in patients with malignant bone lesions can present higher errors then in healthy patients. The Bland-Altman plots in figures 5(a)–(e) show an overestimation of the hydroxyapatite concentration in the spongiosa region by all image-based quantification. Similar tendency is observed in figures 3(a)–(e) for hydroxyapatite volume fraction quantification in the validation phantom and figures 4(a)–(e) for BMC quantification in whole vertebrae of ESP. This overestimation is larger for the DSCT image-based quantifications. This systematic error might be related to approximations that had to be made due to insufficient information about the detector response function. The DSCT used in this study is a third generation CT of the manufacturer. Two main features were included in this equipment: the first is a tin filter which is used for the high-energy x-ray beam (150 kV) typically used in DEQCT. Primak *et al* (2009) showed that the use of tin (Sn) filters between 0.5 mm and 0.8 mm increases the dual-energy contrast between clinically relevant materials. The second feature is an improved detector collimation by using an anti-scatter 3D collimator grid.

As documented in the methods section, we extracted the detector response function from the publication by Liu *et al* (2009), where a second generation DSCT and a third generation detector were used. Therefore, it is expected that these two detector response functions do not exactly match. A similar problem lies in the SOMATOM Scope CT (Siemens Healthineers 2018) that is integrated in the SPECT/CT, which uses an ultra-fast ceramics detector, also corresponding to the manufacturer's second generation (Ulzheimer and Freund 2018). The fact that the SPECT/CT-based quantification of hydroxyapatite showed better results than the DSCT-based may be due to a better characterization of the x-ray beam and detector of the SPECT/CT system.

Furthermore, in Bland-Altman plots (figures 5(a)–(e)), the Qr40 and I41s based quantification show intervals of confidence smaller than Br59 based quantification. Therefore, they provide a more precise measurement of the BMD in spongiosa. The I41s based quantification show a bias smaller than Qr40 and Br59 based quantification. This indicates that I41s based quantification provides a more accurate measurement of the BMD in spongiosa. Also, for the Qr40 and I41s based quantification the mean difference decreases with the increase of BMD. This tendency is inverted in Br59 based quantification and it is similar to the observation presented in figures 4(a)–(e).

Clinical application of mass fraction method in a patient image set

The comparison of DEXA- and DSCT-based BMC quantification in lumbar vertebrae 1 and 2 provides an important means of validating both quantification techniques in the clinical routine. In our study to compare the same parameter, we focused on BMC quantification. Regarding the obtained relative errors (7.6% and −8.4%), a good quantification of lumbar vertebrae 1 and 2 was achieved. Patient positioning represents a potential source of error. In DEXA studies, lumbar vertebrae are positioned parallel to the patient bed using a padded box. Figure 2 shows an uncorrected vertebra curvature in the DSCT image.

The bone volume fraction was calculated in the patient image set. In previous steps of this study the mass fraction method was validated by the quantification of the hydroxyapatite volume fraction in the phantom experiment. Yet, the quantification of bone volume fraction was the principal goal of this study. The quantification of marrow cellularity using MR imaging, as it was applied in a previous study by our group (Salas-Ramirez *et al* 2018), and trabecular bone volume fraction using DEQCT (Wilderman *et al* 2013, Goodsitt *et al* 2014) are essential to calculate the bone marrow absorbed dose based on a 3D radiation transport model (Shah *et al* 2005, Hough *et al* 2011, O'Reilly *et al* 2016, Geyer *et al* 2017). This 3D radiation transport model of bone marrow used trabecular bone microstructures to reproduce the bone spatial distribution in spongiosa. In these studies, the microstructures were obtained from a specific skeletal site of a human cadaver. Therefore, they represent a specific trabecular bone volume fraction (or bone volume fraction in spongiosa). In contrast, the quantification of patient-specific trabecular bone volume fraction using DEQCT will permit to adjust the microstructure of trabecular bone to a patient undergoing molecular radiotherapy.

In this study we propose two methods to calculate bone volume fraction: (i) to use a reference ratio of mineral bone mass fraction to total bone mass fractions ($R_{\mathrm{HA/B}}$) and (ii) to change from hydroxyapatite chemical description to cortical bone chemical description (ICRU report 44 (White 1989)) in the material definition used in the mass fraction method.

The bone volume fraction calculation based on a reference ratio of mineral bone to total bone mass fractions ($R_{\mathrm{HA/B}}$) is easy to implement, because it is based on the quantification of hydroxyapatite mass fraction. However, there is a lack of values for many bone sites and in the best of our knowledge, only the study of Quelch *et al* (1983) provides information about the percentage by mass of mineral bone in a human vertebra.

The change of the chemical description of the quantified material specifically hydroxyapatite to cortical is also easy to implement and provides a better patient-specific assessment. The principal disadvantage of this approach is the grade of agreement between the chemical composition of bone (ICRU report 44 (White 1989)) and the chemical composition of bone in an individual patient.

Although both approaches require general assumptions, the second approach provides a better patient-specific assessment.

In our patient study, we measured the hydroxyapatite mass fraction, hydroxyapatite volume fraction, bone mass fraction, the bone volume fraction and the ratio of mineral bone mass fraction to total bone mass fraction ($R_{\mathrm{HA/B}}$) by using both calculation methods. The $R_{\mathrm{HA/B}}$ values were lower than the value (0.663) reported by Quelch *et al* (1983). Which quantified the mineral content in dry, fat-free bone samples. Therefore, it is expected that the quantification of bone volume fraction by the first method (based on a reference ratio of mineral bone to total bone mass fraction) overestimates the bone volume fraction due to the lack of water content in the calculation. In table 5, the bone volume fraction obtained by using a reference ratio of mineral bone to total bone mass fraction provided larger bone volume fractions than the second method (change of material definition—hydroxyapatite to cortical bone).

Also, in table 5, it is possible to see that hydroxyapatite mass fraction values are smaller than bone mass fraction values. This result is in agreement with the bone composition (mineral bone plus organic material). The

values of the ratio of mineral bone to total bone mass fraction remain almost constant at 0.554 to 0.558 for both regions (whole vertebra and spongiosa) and smaller than the value report by Quelch *et al* (1983). This difference might by related with water content in the patient's vertebra.

Lastly, the bone volume fraction is higher in the whole vertebra than in the spongiosa. This result is in agreement with the spatial distribution of bone in vertebrae, as cortical bone (high concentration of bone) plus trabecular bone (low concentration of bone) are considered when looking at whole vertebrae.

The International Commission of Radiation Protection (ICRP) in the report 70 (ICRP 2002) documented the portion of spongiosa occupied by trabecular bone (trabecular bone volume fraction) measured by Arnold and Wei in adult vertebrae. They documented values of 0.114 in adults at ages between 51–60 years, 0.085 in adults at ages between 61–80 years and 0.077 in adults at ages between 81–90 years. The patient's bone volume fraction in spongiosa (of both calculation methods) are lower than the values documented by Arnold and Wei (1972). This result might be related with the patient diagnosis of osteopenia.

Study limitations

Geyer *et al* (2017) explored the effect of changes in bone mineral density ($\pm5\%$, $\pm10\%$ and $\pm15\%$) on *S* values for three bone sites (ribs, lumbar vertebra 3 and parietal bone). For lumbar vertebra 3, the *S* value corresponding to the irradiation of trabecular bone volume to active marrow for 4 of 6 investigated radionuclides (^{45}Ca, ^{223}Ra, ^{219}Rn, and ^{215}Po) showed a change with respect to the reference S value equal to or larger than $\pm10\%$. For the other two radionuclides (^{153}Sm and ^{90}Y), changes below 10% were found. These changes lie in the order of the maximum expected quantification relative errors obtained in our study (5.4%—SPECT/CT and 10%—DSCT) for a bone mineral (hydroxyapatite) density $\geqslant 200\,\mathrm{g\,cm^{-3}}$ in spongiosa. This indicates that, for lumbar vertebrae, the relative error of the presented method has to be further reduced before it significantly affects S value calculations.

The phantom geometry was limited to the vertebral geometry. However, the beam hardening effect is expected to be more important in regions as parietal bone, femoral heads, hips and humeral heads. A test of the mass fraction method in conjunction with the method proposed by Goodsitt *et al* (1991, 2014) in these anatomical regions could validate the use of the mass fraction method under different beam hardening conditions.

Lastly, the ESP dimensions do not represent all the diversity of patient sizes. Therefore, a study with other phantom thicknesses could potentially provide more size-independent information on the mass fraction method's performance.

Conclusion

Our study shows that DEQCT using the phantomless mass fraction method represents a technique with sufficient accuracy to quantify HA in a clinical setting. An overestimation of the hydroxyapatite volume fraction was observed in all quantified regions, in particular in the spongiosa region of ESP. This observation might be related to approximations that had to be made due to insufficient information about the x-ray spectra and the detector sensitivity function. This method requires an adequate characterization of the x-ray beam and the detector. It is also sensitive to the reconstruction kernel and chemical description of reference materials. In the spongiosa region the agreement between SPECT/CT-based quantification and the European Spine Phantom nominal values is better than the agreement between DSCT-based and ESP nominal values, which can be attributed to a better description of the x-ray beam and detector for the SPECT/CT system. Therefore, the SPECT/CT provides a clinical approach for DEQCT when using the mass fraction method in our clinical setting.

With this method, it is possible to quantify the bone volume fraction in spongiosa which is equivalent to TBVF directly with a SPECT/CT in a nuclear medicine department. Therefore, it provides valuable input to a computational model for obtaining patient-specific values of TBVF in lumbar vertebrae. Subsequent studies should be performed to evaluate the performance of the mass fraction method in different anatomical regions.

Acknowledgments

References

Arnold J S and Wei L T 1972 Quantitative morphology of vertebral trabecular bone *Radiobiology of Plutonium* ed B Stover and W S S Jee (Salt Lake City, UT: J.W. Press) pp 333–54
Azevedo S G *et al* 2016 System-independent characterization of materials using dual-energy computed tomography *IEEE Trans. Nucl. Sci.* **63** 341–50

Bolch W, Patton W, Rajon D, Shah A, Jokisch D and Inglis B 2001 Considerations of marrow cellularity in 3-dimensional dosimetric models of the trabecular skeleton *J. Nucl. Med.* **43** 97–108

Booz C *et al* 2017 Evaluation of bone mineral density of the lumbar spine using a novel phantomless dual-energy CT post-processing algorithm in comparison with dual-energy x-ray absorptiometry *Eur. Radiol. Exp.* **1** 11

Christel T, Kuhlmann M, Vorndran E, Groll J and Gbureck U 2013 Dual setting alpha-tricalcium phosphate cements *J. Mater. Sci. Mater. Med.* **24** 573–81

Emami A *et al* (ed) 2011 A new phantom for performance evaluation of bone mineral densitometry using DEXA and QCT *2011 IEEE Nuclear Science Symp. Conf. Record (23–29 October 2011)*

Fedorov A *et al* 2012 3D Slicer as an image computing platform for the Quantitative Imaging Network *Magn. Reson. Imaging* **30** 1323–41

Geyer A M, Schwarz B C, Hobbs R F, Sgouros G and Bolch W E 2017 Quantitative impact of changes in marrow cellularity, skeletal size, and bone mineral density on active marrow dosimetry based upon a reference model *Med. Phys.* **44** 272–83

Goodsitt M M *et al* 2014 Evaluation of dual energy quantitative CT for determining the spatial distributions of red marrow and bone for dosimetry in internal emitter radiation therapy *Med. Phys.* **41** 051901

Goodsitt M M, Johnson R H and Chesnut C H 3rd 1991 A new set of calibration standards for estimating the fat and mineral content of vertebrae via dual energy QCT *Bone Miner.* **13** 217–33

Heismann B J, Leppert J and Stierstorfer K 2003 Density and atomic number measurements with spectral x-ray attenuation method *J. Appl. Phys.* **94** 2073–9

Hindorf C, Glatting G, Chiesa C, Linden O and Flux G 2010 EANM Dosimetry Committee guidelines for bone marrow and whole-body dosimetry *Eur. J. Nucl. Med. Mol. Imaging* **37** 1238–50

Hines C D, Yu H, Shimakawa A, McKenzie C A, Brittain J H and Reeder S B 2009 T1 independent, T2∗ corrected MRI with accurate spectral modeling for quantification of fat: validation in a fat-water-SPIO phantom *J. Magn. Reson. Imaging* **30** 1215–22

Hough M, Johnson P, Rajon D, Jokisch D, Lee C and Bolch W 2011 An image-based skeletal dosimetry model for the ICRP reference adult male—internal electron sources *Phys. Med. Biol.* **56** 2309–46

ICRP 1995 Basic anatomical and physiological data for use in radiological protection: the skeleton *Ann. ICRP* **25** 1–80

ICRP 2002 Basic anatomical and physiological data for use in radiological protection: reference values *Ann. ICRP* **32**

International Atomic Energy Agency NDSV 1998 XMuDat: Photon attenuation data on PC Version 1.0.1 of August 1998 Summary documentation. Retrieved from International Atomic Energy Agency (IAEA) (http://inis.iaea.org/search/search.aspx?orig_q=RN:30022813)

Kalender W A 1992 A phantom for standarization and quality control in spinal bone mineral measurements by QCT and DXA: design considerations and specifications *Med. Phys.* **19** 583–6

Kikinis R, Pieper S D and Vosburgh K G 2014 3D Slicer: A platform for subject-specific image analysis, visualization, and clinical support *Intraoperative Imaging and Image-Guided Therapy* ed F Jolesz (New York, NY: Springer)

Lipton A *et al* 2009 The science and practice of bone health in oncology: managing bone loss and metastasis in patients with solid tumors *J. Natl Compr Canc. Netw.* **7** S1–29; quiz S30

Liu X, Yu L, Primak A N and McCollough C H 2009 Quantitative imaging of element composition and mass fraction using dual-energy CT: three-material decomposition *Med. Phys.* **36** 1602–9

Neuman W 1980 Bone material and calcification mechanisms *Fundamental and Clinical Bone Physiology* ed M R Urist (Philadelphia, PA: J. B. Lippincott Co.) pp 83–107

O'Reilly S E *et al* 2016 An image-based skeletal dosimetry model for the ICRP reference adult female-internal electron sources *Phys. Med. Biol.* **61** 8794–824

Primak A N, Ramirez Giraldo J C, Liu X, Yu L and McCollough C H 2009 Improved dual-energy material discrimination for dual-source CT by means of additional spectral filtration *Med. Phys.* **36** 1359–69

Quelch K J, Melick R A, Bingham P J and Mercuri S M 1983 Chemical composition of human bone *Arch. Oral Biol.* **28** 665–74

R Core Team 2008 R: A language and environment for statistical computing. R Foundation for Statistical Computing, Vienna, Austria (http://www.R-project.org/)

Salas-Ramirez M *et al* 2018 Quantification of fat fraction in lumbar vertebrae: correlation with age and implications for bone marrow dosimetry in molecular radiotherapy *Phys. Med. Biol.* **63** 025029

Schindelin J *et al* 2012 Fiji: an open-source platform for biological-image analysis *Nat. Methods* **9** 676–82

Schneider C A, Rasband W S and Eliceiri K W 2012 NIH Image to ImageJ: 25 years of image analysis *Nat. Methods* **9** 671–5

Shah A, Bolch W, Rajon D, Patton P and Jokisch D 2005 A paired-image radiation transport model for skeletal dosimetry *J. Nucl. Med.* **46** 344–53

Simens Healthineers 2018 *Simulation of X-ray Spectra* Online tool for the simulation of x-ray Spectra (https://oem-xray-components.siemens.com/x-ray-spectra-simulation)

Thomsen J S, Jensen M V, Niklassen A S, Ebbesen E N and Bruel A 2015 Age-related changes in vertebral and iliac crest 3D bone microstructure—differences and similarities *Osteoporos. Int.* **26** 219–28

Ulzheimer S and Freund J 2018 The stellar detector *White Paper* (Siemens) (https://www.siemens-healthineers.com/computed-tomography/technologies-innovations/stellar-detector)

White D R, Booz J, Griffith R V, Spokas J J and Wilson I J 1989 Report 44: tissue substitutes in radiation dosimetry and measurement *J. of the ICRU* **os23** 1

Wilderman S J, Roberson P L, Bolch W E and Dewaraja Y K 2013 Investigation of effect of variations in bone fraction and red marrow cellularity on bone marrow dosimetry in radio-immunotherapy *Phys. Med. Biol.* **58** 4717–31

Woodard H Q and White D R 1982 Bone models for use in radiotherapy dosimetry *Br. J. Radiol.* **55** 277–82